Eur. Phys. J. Appl. Phys. (2012) 60: 31101
DOI: 10.1051/epjap/2012120128

THE EUROPEAN PHYSICAL JOURNAL APPLIED PHYSICS

Regular Article

Investigating the confining compressibility of STF at high deformation rate

Weifeng Jiang[1], Xinglong Gong[1,a], Yulei Xu[1], Shouhu Xuan[1], Wanquan Jiang[2], Wei Zhu[2], Xiaofeng Li[1], and Lijun Qin[1]

[1] CAS Key Laboratory of Mechanical Behavior and Design of Materials, Department of Modern Mechanics, University of Science and Technology of China (USTC), Hefei 230027, P.R. China
[2] Department of Chemistry, USTC, Hefei 230026, P.R. China

Received: 4 April 2012 / Received in final form: 14 September 2012 / Accepted: 14 November 2012
Published online: 12 December 2012 –

Abstract. The split Hopkinson pressure bar (SHPB) was used to study the compressibility of shear thickening fluid (STF) at high deformation rate. In this study, a steel bulk was introduced into the SHPB system to confine and load the STF. A series of STFs with different particle types (SiO_2 and PSt-EA) and volume fractions (63 vol.% and 65 vol.%) were tested and the results were compared. The reliability of the results was proved by repeating the tests and the force balance in suspension. The bulk modulus was used to evaluate the compressibility of STF, which indicated that the SiO_2-based STF exhibited a larger compressibility than the PSt-EA-based STF. It was found that the bulk modulus increases with increasing of the strain rate and the volume fraction shows little effect on the bulk modulus. The structure-dependent mechanical property was analyzed and the loading effect of bulk modulus was considered to be originated from the interparticle clustering.

1 Introduction

Shear thickening fluid (STF) is a monodisperse suspension of colloidal particles, whose viscosity will sharply change when encountering a large enough disturbance [1]. Such a viscosity change phenomenon was defined as shear thickening behavior and several different thickening statuses have been found. The extensional viscosity increases sharply with increasing of the extensional rate [2]. Sudden stiffening under dynamic squeezing flow similar to shear thickening effect was also found [3]. Due to the intrinsic advantages of the thickening behavior, the STF was working without consuming external energy. Therefore, they have attracted in lots of applications, such as a damper [4], body armor [5–7], sandwiched beam for vibration control [8] and hip padding system [9].

Numerous researches have been dedicated to understanding the mechanical properties of STF. Besides the phase volume, particle size and particle shape, it was found that the microstructure of the arranged particles also highly influenced the fluid mechanics and rheology of the concentrated STF suspension [10]. Hoffman pointed out that the particles transform from two-dimension layered arrangement in low shear rate to random arrangement when the critical shear rate reached (ODT) [11,12], thus the shear thickening arises from the rearrangement of internal particles. Based on the simulation, Brady and Bossis assumed that the formation of the particles clusters after ordered arrangement was the origin for the shear thickening effect [13]. Flow-small angle neutron scattering measurements also indicated the reason for shear thickening was due to the hydrodynamic clustering [14–17]. Recently, Cheng et al. directly observed clustering during thickening by a homemade confocal rheometer [18]. Lee and Wagner found that the critical strain required for thickening to form depended inversely on frequency at low frequency. Unfortunately, the result at high frequency was not easily measured due to the wall slip [19]. Fischer et al. found that the relationship of critical strain and frequency followed a unique-power-law in pre- and post-transition state [20]. In addition, the extensional rheology of STF was tested by using a homemade filament-stretching rheometer and the magnitude of strain hardening was observed when reaching a critical extension rate [2].

However, most of the above works were focused on the low deformation rate-shear rheology, the mechanical properties of the STF under high deformation rate remain unclear. The STF device often encounters high-strength impact and the deformation rate is very large [5–7]. The mechanical property at high deformation rate is different from static condition, such as aluminum alloy foams [21], steel fiber-reinforced concrete [22] and live cell cultures [23]. Therefore, the mechanical property of the

[a] e-mail: gongxl@ustc.edu.cn

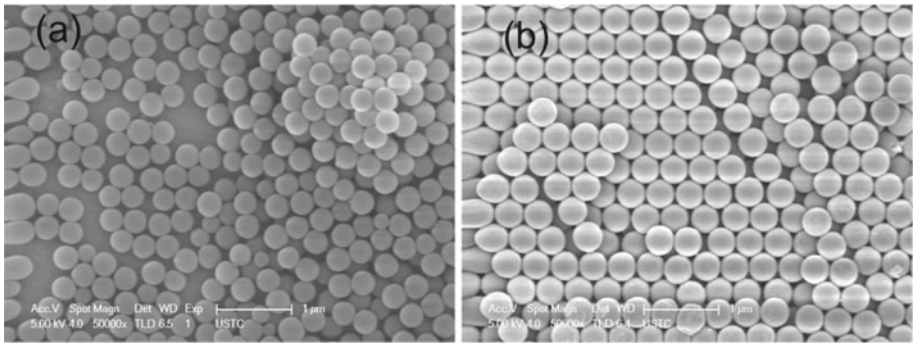

Fig. 1. (a) SEM image of the SiO_2 particles, (b) SEM image of the PSt-EA particles.

STF at high strain rate was urgently required. Recently, Hopkinson bar has been widely applied to test viscous materials under high deformation rate [24]. Lim et al. conducted a lot of works on testing viscous liquid by SHPB. They firstly detailed the testing condition of the viscous fluid [25] and then the rheology of STF under dynamic squeezing flow was obtained. They found that the STF exhibited thickening during the extrusion and the dependence of the lording rate on the transitional time was discussed [3]. At last, a phenomenological modeling which was based on the dynamic squeezing flow was developed [26].

In this work, the compressibility of STF is investigated by using the SHPB to fully understand the transient properties of STF under high deformation rate. The bulk modulus is used to evaluate the compressibility of STF. The influencing factor of the bulk modulus was presented and discussed in terms of the experimental data, such as volume fraction, particle type and loading rate. The loading rate effect of bulk modulus for different suspension will be discussed.

2 Material and experimental method

2.1 Shear thickening fluid

The shear thickening fluid was traditionally composed of monodisperse colloidal particles and a carrier fluid. The colloidal particles evaluated in this study consisted of SiO_2 and PSt-EA, and the carrier fluid was ethylene glycol. The volume fraction was kept at 63 vol.% and 65 vol.%, respectively. The SiO_2 and PSt-EA particles were measured by scanning electron microscope (SEM, Fig. 1) and the size of the particles was 250 nm and 350 nm, respectively.

2.2 Split Hopkinson pressure bar

A classical SHPB setup consists of a striker bar, an incidence and a transmission bar, while a specimen is sandwiched between the incident bar and the transmmission bar. The schematic diagram and the basic parameters of SHPB used in this study are shown in Figure 2 and Table 1 respectively. During testing, the striker bar which is fired out of a gas gun impacts the incident bar and an elastic wave as a function of time $\varepsilon_{\mathrm{I}}(t)$ is produced. The elastic wave propagates through the incident bar then reaches the specimen-bar interface. Because the wave impedance of incident bar is different from the specimen, a fraction of this pulse is reflected back as a tensile pulse $\varepsilon_{\mathrm{R}}(t)$ and the rest is transmitted through the specimen as a compressive pulse $\varepsilon_{\mathrm{T}}(t)$. The strain gages were placed in both the incident bar and transmission bar, so that these strain amplitudes ($\varepsilon_{\mathrm{I}}(t)$, $\varepsilon_{\mathrm{R}}(t)$ and $\varepsilon_{\mathrm{T}}(t)$) can be recorded by an amplifier and an oscillograph. The surface force in front of specimen P_{f}, the surface force in back of specimen P_{b} and the strain rate of specimen can be obtained by the one-dimensional elastic stress wave theory.

$$\begin{aligned} P_{\mathrm{f}}(t) &= \left[\varepsilon_{\mathrm{I}}(t) + \varepsilon_{\mathrm{R}}(t)\right] A_{\mathrm{b}} E_{\mathrm{b}} \\ P_{\mathrm{b}}(t) &= A_{\mathrm{b}} E_{\mathrm{b}} \varepsilon_{\mathrm{T}}(t) \\ \dot{\varepsilon}(t) &= \frac{C_{\mathrm{b}}}{T_{\mathrm{S}}} \left[\varepsilon_{\mathrm{I}}(t) - \varepsilon_{\mathrm{R}}(t) - \varepsilon_{\mathrm{T}}(t)\right]. \end{aligned} \tag{1}$$

Assume that the axial force in specimen reaches balance, i.e., $P_{\mathrm{f}} = P_{\mathrm{b}}$.

$$\begin{aligned} \sigma(t) &= \frac{P_{\mathrm{f}} + P_{\mathrm{b}}}{2A_{\mathrm{S}}} = E_{\mathrm{b}} \varepsilon_{\mathrm{T}}(t) \\ \dot{\varepsilon}(t) &= -\frac{2C_{\mathrm{b}}}{T_{\mathrm{S}}} \varepsilon_{\mathrm{R}}(t) \\ \varepsilon(t) &= -\frac{2C_{\mathrm{b}}}{T_{\mathrm{S}}} \int_0^T \varepsilon_{\mathrm{R}}(t) \mathrm{d}t, \end{aligned} \tag{2}$$

where A_{b} and A_{S} are the cross-sectional areas of the bars and the specimen, respectively; E_{b} is the elastic modulus of the bar; C_{b} is the sound velocity of the bar; T_{s} is the thickness of the specimen and T is the pulse length. In this study, the cross-sectional areas of both the bars and the specimen are equal ($A_{\mathrm{b}} = A_{\mathrm{S}}$). This is the traditional method of data processing in SHPB, and the stress, the strain rate and the strain are provided here as engineering values.

3 Experimental results

3.1 Effect of the bulk

A bulk consisting of a cylindrical container (steel) and two pistons (aluminum) is used to confine and load the

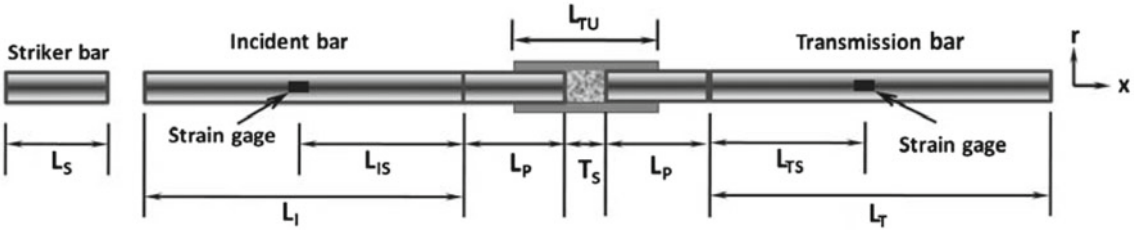

Fig. 2. Split Hopkinson pressure bar experimental schematic.

Table 1. Split Hopkinson pressure bar basic parameters.

Parameter		
Incident bar length	L_{I}	0.86 m
Transmission bar length	L_{T}	0.48 m
Piston length	L_{P}	0.03 m
Incident bar diameter	D_{I}	0.0145 m
Transmission bar diameter	D_{T}	0.0145 m
IB strain gage distance from specimen	L_{IS}	0.43 m
TB strain gage distance from specimen	L_{TS}	0.24 m
Bar elastic modulus	E_{b}	65.4 GPa
Bar density	ρ_{b}	2700 kg/m^3
Measured sound velocity (IB)	C_{b}	5050 m/s
Striker bar diameter	D_{S}	0.0145 m
Striker bar length	L_{S}	0.15 m
Specimen thickness	T_{S}	0.005 m
Container length	L_{TU}	0.04 m
Container elastic modulus	E_{B}	210 GPa

STF (Fig. 2) [23,27,28]. The clearance between the pistons and the container is filled with vaseline for two advantages: The first advantage is that the vaseline is used as a lubrication to reduce the container-pistons friction. The second advantage is that the vaseline prevents the leak effectively. It is the difference between our work and Lim's investigation [25]. In Lim's study, the specimen is covered by a flexible band. The pressure developed by the band is found to be two orders of magnitude lower than pressures associated with the Hopkinson bar experiments, indicating that the lateral deformation is not limited and the STF is under dynamic squeezing flow. However, in our study the STF is put into the steel bulk and the lateral deformation is limited. The STF loading was under a confined compression. When the bulk was undergoing a lateral force, the accuracy of the testing results was affected a little due to the expansion of the container. Therefore, it is important to determine whether the lateral deformation can be neglected. Assuming that the lateral force of bulk is equal to the axial force of specimen, i.e., $\sigma_x = \sigma_r$; x and r are the coordinates defined in Figure 2 [28]. The entire loading of the steel bulk is in the elastic range. According to the elasticity theory, the lateral displacement $u(r)$ is determined by the equation:

$$u(r)/_{r=a} = \frac{a^2\sigma_r}{E_{\mathrm{B}}(b^2-a^2)}\left[\frac{(1+v)b^2}{a} + (1+v)a\right], \quad (3)$$

where $\nu = 0.3$ is the Poisson ratio of the steel, $E_{\mathrm{B}} = 210$ GPa is the elastic modulus of the container, $a = 7.3$ mm and $b = 12.5$ mm are the inner radius and outer radius of the cylindrical container. The value of $u(r)/_{r=a}$ is equal to 8.13×10^{-3} mm, when the σ_r is set at 100 MPa. Since this value is sufficiently small in comparison to the value of inner radius $a = 7.3$ mm, the container can be regarded as a rigid container. Thus, it is considered that there is no lateral deformation of specimen. Several difficulties are encountered in determining the thickness of the STF. When the thickness of the STF sample is large, the transmission signal is too weak to be measured. However, the homogeneity of the STF sample is bad if the thickness is too small. When the STF thickness is greater than 1000 times the particle diameter, the STF can be defined as a homogeneous sample during the mechanical testing [3]. Therefore, based on our pre-experiments, the thickness of the STF is set at 5 mm in this work.

3.2 Dynamic equilibrium and repeatability of SHPB experiment

In the dynamic SHPB experiment, the test results should be repeated and the dynamic equilibrium state should be established. Then the experiment is considered valid. Two specimens were tested in the same condition (the ambient temperature is 23 ± 0.5 °C, the speed of striker bar is 19.6 m/s) and the recorded pulses are shown in Figure 3. Obviously, the incident pulse, reflected pulse and transmission pulse are nearly identical. The two waveforms were repeated well, thus the repeatability of the results is very good.

The force in the suspension should be balanced. In other words, the force of each cross-section of the STF was uniform. However, due to the limitation of the present experimental technique, the specimens were considered in equilibrium state, when the forces on both force end and the back end of the STF were equal. There are two methods to verify the dynamic equilibrium: one is directly measuring the surface force by using quartz gages [29]. Another one is using the elastic wave theory by considering that the front surface force is equal to the sum of the incident force and reflected force, and the back surface force is equal to the transmitted force. Due to the difficulty of the quartz gage installation in our testing system, the second method was selected to test the STF although the first method is more accurate than the second one. The STF is considered to be in balance after a ring up time, where

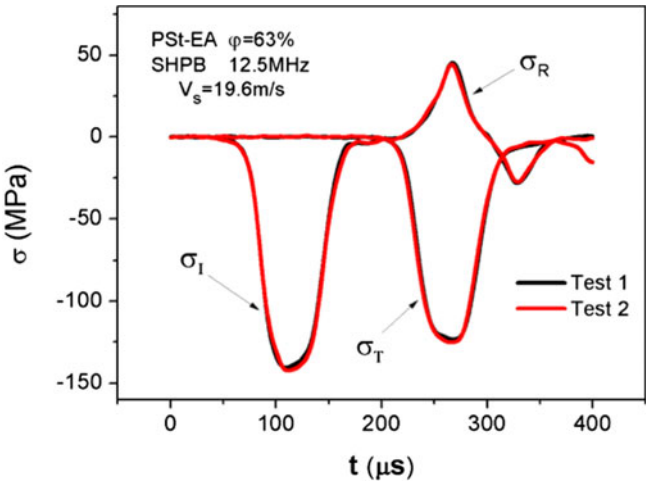

Fig. 3. (Color online) Testing the 63 vol.% PSt-EA suspension under the same condition (the ambient temperature is 20 ± 0.5 °C, the sampling frequency is 12.5 MHz, the speed of striker bar is 19.6 m/s).

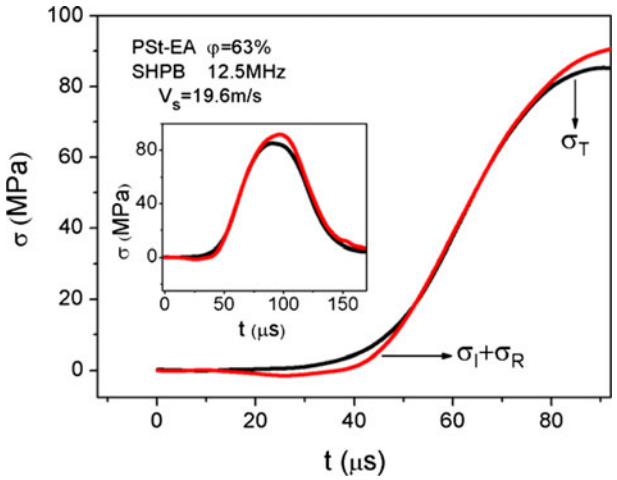

Fig. 4. (Color online) The force balance in STF for 63 vol.% PSt-EA suspension.

the ring up time is the transit time for the stress wave traveling through the STF for 3–4 times, and it is shown in the initial period of the loading in Figure 4 [30]. A pulse shaper which increases the loading time is placed on the impact surface of the incident bar, ensuring enough time for force balance in the STF [31,32]. The front surface stress ($\sigma_{\mathrm{I}} + \sigma_{\mathrm{R}}$) almost coincides with the back surface stress (σ_{T}) in the loading procedure, indicating that the STF is in balance. In this study, only the data in the loading is used, thus the unbalance state of the force during the unloading does not show any influence on our research. The force unbalance may be caused by the dissipated energy which will be presented and discussed in the following analysis.

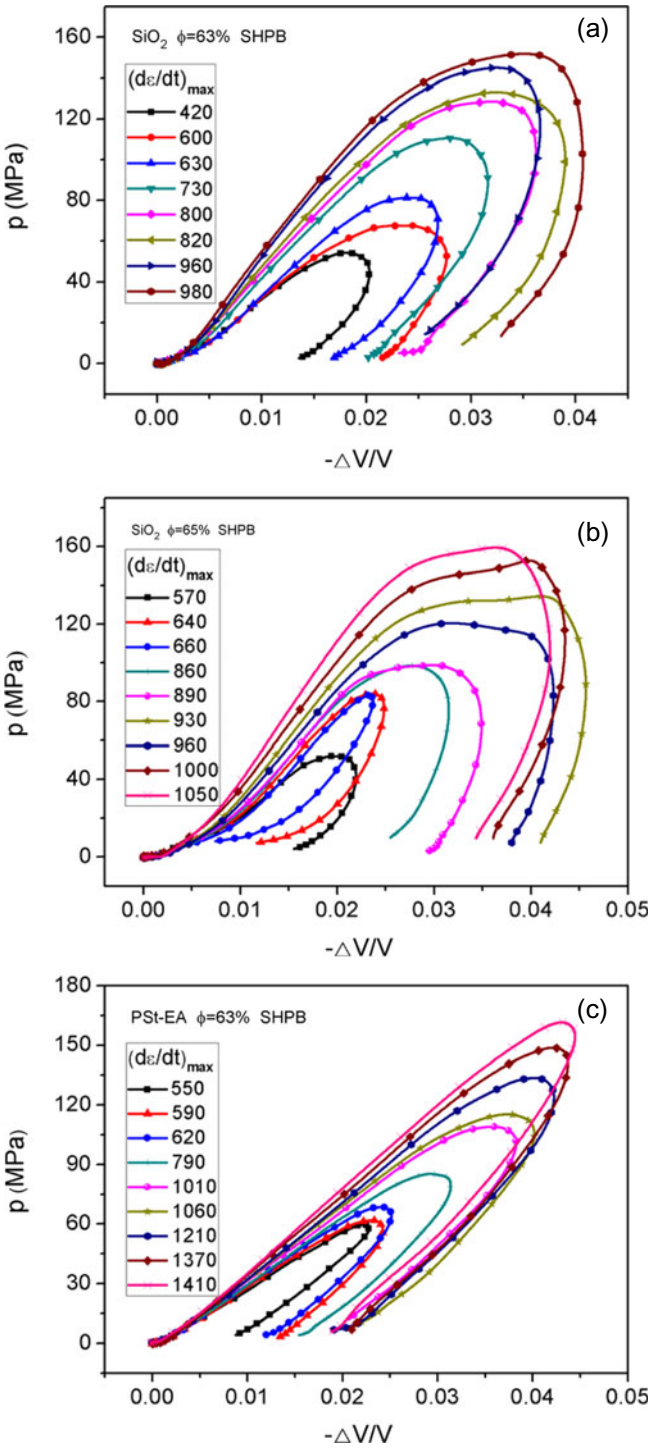

Fig. 5. (Color online) The axial pressure p as a function of $-\Delta V/V$ for (a) 63 vol.% colloidal suspension of SiO_2, (b) 65 vol.% colloidal suspension of SiO_2 and (c) 63 vol.% colloidal suspension of PSt-EA in the ethylene glycol under different strain rates by the SHPB technique.

3.3 Effect of strain rate

In Figure 5, the axial pressure p is presented as a function of the volume change ($-\Delta V/V$) for the three STF suspensions. The strain rates were obtained by adjusting the

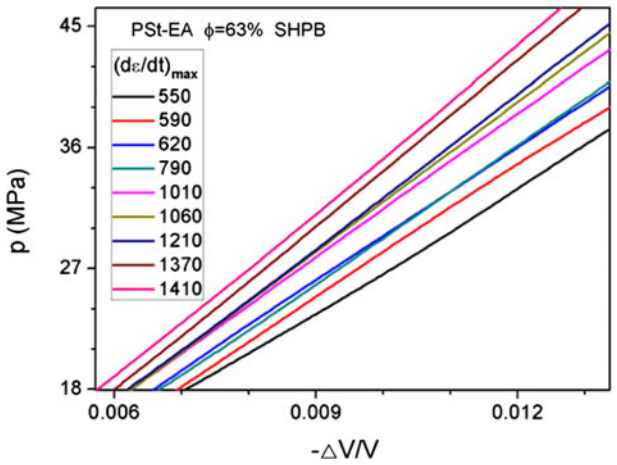

Fig. 6. (Color online) The axial pressure p as a function of $-\Delta V/V$ which enlarged loading segment for 63 vol.% PSt-EA suspension in ethylene glycol.

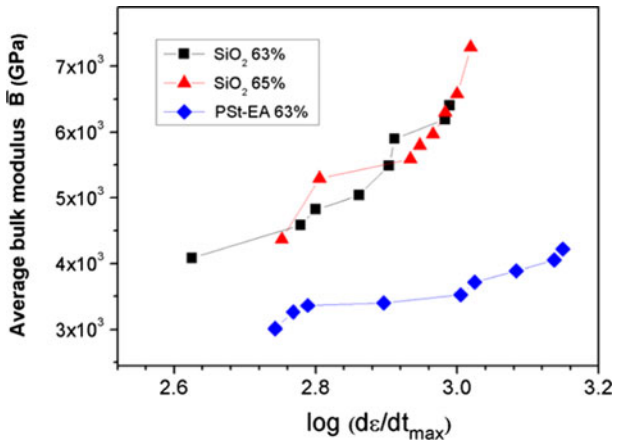

Fig. 7. (Color online) The average bulk modulus as a function of the maximum logarithmic strain rate for three different types of STFs.

pressure of the air gun. The maximum strain rate is used to describe the loading rate in this study, because the constant strain rate does not present in the experimental results. The σ-ε curve which describes the one-dimensional stress state is not used because the specimen is in the three-dimensional stress state under the lateral restraint. Based on the precious analysis, the lateral deformation of the steel container can be neglected, so it can be achieved that $p = \sigma$, $\Delta V/V = \varepsilon$. Note that σ and ε are calculated by equation (2).

The compressibility of air is much larger than the STF's. If the STF mixes with air, the volume is changed by the deformation of both the air and the STF, and the deformation of the air plays a dominant role in total volume deformation. Thus the accuracy of the strain rate and the strain will be affected. In order to remove the air, the STFs are consecutively degassed three times by ultrasound instrument, and each time sustains 10 h. The nonlinearity which is caused by the air evidently appears in the initial curve (Fig. 5). However, the air has been removed as much as possible in this study. In Figure 5, it is clear that higher pressures are generated for higher strain rate and each of the curves follows a same trend. During loading, the nonlinearity which has been discussed appears in the initial period of deformation. With increasing of the pressure p, the p-$(-\Delta V/V)$ curve transforms to near linearity. Then, it comes back to nonlinearity again, when the pressure p is close to the maximum value. Finally, the rebound phenomenon is found in the unloading, because parts of the compressed volume of the STF are returned. According to the Hopkinson technique, the trend of the reflected wave is same as the trend of the volume change rate ($\mathrm{d}\varepsilon/\mathrm{d}t = \mathrm{d}(\Delta V/V)/\mathrm{d}t$). The amplitude of the reflected wave (σ_R) changes from positive to negative (Fig. 3). Therefore, the volume change rate also changes from negative to positive, indicating the existence of the rebound phenomenon.

The loading portion of the p-$(-\Delta V/V)$ curve is shown in Figure 6 for the STF prepared by 63 vol.% of PSt-EA. It is found that the slope of the curve increases with the maximum strain rate. The slope of the curve is defined as the bulk modulus B which determines the degree of compressibility of the STF. It is similar to the elastic modulus which describes the uniaxial compressibility of solid. In Figure 6, it is clear that the bulk modulus of the STF relates to the strain rate. The results in this study are different from those of Lim's investigation [25]. In Lim's studies, the strain rate influences the transition time which defines the period during when jamming occurs and the onset and end of deceleration. The strain rate effect of the bulk modulus of STF will be presented and described in the discussion.

4 Discussion

The average bulk modulus as a function of the maximum logarithmic strain rate is obtained by using the results of Figure 5 and is plotted in Figure 7. Because the curve in loading region is not ideal linearity and the different points have different slopes, in this study the average bulk modulus B was obtained by calculating the average value of the slopes of the curves in the loading region. In Figure 7, we find that the average bulk modulus of STF is influenced by the volume fraction, particle type and strain rate.

To investigate the influence of volume fraction, the functions in same particle SiO_2 but in different volume fraction (63 vol.% SiO_2 and 65 vol.% SiO_2 suspension) are plotted in Figure 7. It is clear that the average bulk modulus of the 63 vol.% SiO_2 suspension and the 65 vol.% SiO_2 suspension is similar in the same maximum strain rate, indicating that the volume has less effect on the average bulk modulus of the STF. The influence of particle type is obtained by comparing the suspension of the SiO_2 particles with the suspension of the PSt-EA particles in the same volume fraction. The hardness of SiO_2 particle is greater than the one of PSt-EA particle. The average bulk modulus of the 63 vol.% SiO_2 suspension is greater than the 63 vol.% PSt-EA suspension. As a result, it can be concluded that the particles with a larger hardness exhibit a larger average bulk modulus.

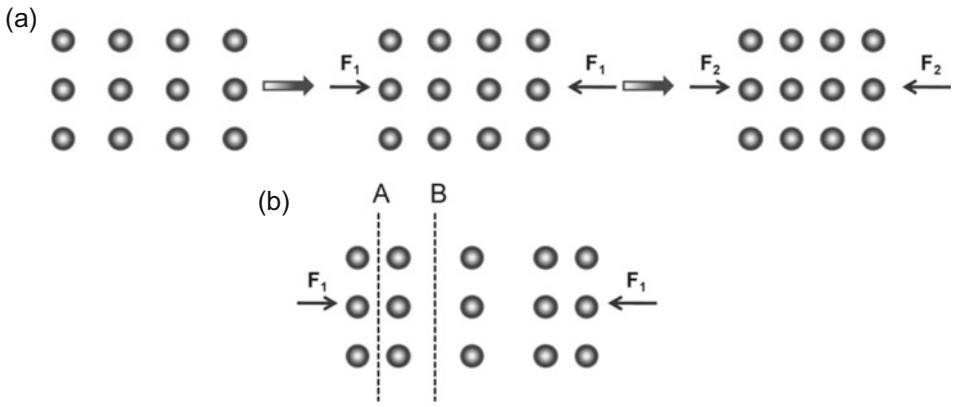

Fig. 8. (a) The deformation between internal atoms when loading rate is small, (b) deformation between internal atoms when loading rate is great.

The strain rate effect of the bulk modulus has been qualitatively introduced above. Each date line in Figure 7 shows that the average bulk modulus increases with increasing of the strain rate. The effect of the strain rate on the bulk modulus indicates that the STF becomes harder as the stain rate increases, while the shear thickening effect indicates that the STF becomes more viscous with increasing of the stain rate. The similarity between these effects is that the STF becomes hard due to deformation as the increase of the deformation rate. The physical phenomenon of the suspension was highly influenced by the microstructure. As previously mentioned, the shear thickening was believed to be a result of particle rearrangement and hydrodynamic clustering formation. Extensive interparticle contacts and clustering are found by Petel and Higgins when the stress wave propagates in dense particle suspensions [33]. The analysis indicates that the difference in compressibility between the particle and the liquid ethylene glycol leads to an evolution of the volume fraction. Thus, the influence of the strain rate on the bulk modulus must be responded for the interparticle clustering. It was believed that the reason for the movement of the particles is the unbalance of the particle during the stress wave which propagates in dense particle suspensions.

For the dynamic materials, the force passes in a particular speed rather than immediately spread from one area to another area under high strain rate [34]. As shown in Figure 8b, the force F_1 reached the A interfaces but did not reach the B interface. If the loading rate is small, the force between atoms has sufficient time to spread. It changes along the distance between the particles (Fig. 8a). However, if the loading rate is very large and the atomic force is too late to pass, the atoms will unbalance and fluctuate. Judging from atomic level, we can consider that the stress waves spread in solid with the continuous fluctuation of the atoms. For this work, the particles are also unbalanced when the stress wave reaches the front surface but does not reach the back surface. Thus we infer that the stress wave propagation in the STF is accompanied by the fluctuation of the internal particle.

5 Conclusions

The transient compressibility of STFs was studied by using a spilt Hopkinson pressure bar. A series of STFs consisting of concentrations of 63 vol.% of SiO_2, 65 vol.% of SiO_2 and 63 vol.% of PSt-EA in the ethylene glycol demonstrate the influencing factors of the average bulk modulus of STF. The SiO_2-based STF exhibits a larger compressibility than the PSt-EA-based STF. It is found that the average bulk modulus increases with increasing of the strain rate and the volume fraction shows little effect on the average bulk modulus. The internal particle motion within carrier is demonstrated when stress wave propagates in STF. The viscous drag is generated by the particle motion; the interparticle clustering is the reason for the effect of strain rate on the bulk modulus. These results are very important for understanding the intrinsic property of the STFs.

Financial supports from the National Natural Science Foundation of China (Grant No. 11125210) and the National Basic Research Program of China (973 Program, Grant No. 2012CB937500) are gratefully acknowledged. The authors also thank Prof. Shisheng Hu of USTC and his students for their help on the experiment and useful discussions on the results.

References

1. H.A. Barnes, J. Rheol. **33**, 329 (1989)
2. M. Chellamuthu, E.M. Arndt, J.P. Rothstein, Soft Matt. **5**, 2117 (2009)
3. A.S. Lim, S.L. Lopatnikov, N.J. Wagner, J.W. Gillespie, Rheol. Acta **49**, 879 (2010)
4. X.Z. Zhang, W.H. Li, X.L. Gong, Smart Mater. Struct. **17**, 035027 (2008)
5. Y.S. Lee, E.D. Wetzel, N.J. Wagne, J. Mater. Sci. **38**, 2825 (2003)
6. Y. Duan, M. Keefe, T.A. Bogetti, B.A. Cheeseman, Compos. Struct. **68**, 331 (2005)

7. T.J. Kang, K.H. Hong, M.R. Yoo, Fiber. Polym. **11**, 719 (2010)
8. C. Fischer, S.A. Braun, P.-E. Bourban, V. Michaud, C.J.G. Plummer, J.-A.E. Manson, Smart Mater. Struct. **15**, 1467 (2006)
9. S.N. Robinovitch, W.C. Hayes, T.A. McMahon, J. Biomech, Eng. Trans. ASME **117**, 409 (1995)
10. J.J. Stickel, R.L. Powell, Annu. Rev. Fluid Mech. **37**, 129 (2005)
11. R.L. Hoffman, Trans. Soc. Rheol. **16**, 155 (1972)
12. R.L. Hoffman, J. Coll. Interf. Sci. **46**, 491 (1974)
13. J.F. Brady, G. Bossis, J. Fluid Mech. **155**, 105 (1985)
14. H.M. Laun, R. Bung, S. Hess, W. Loose, O. Hess, K. Hahn, E. Hadicke, R. Hingmann, F. Schmidt, P. Lindner, J. Rheol. **36**, 743 (1992)
15. J. Bender, N.J. Wagner, J. Rheol. **40**, 899 (1996)
16. B.J. Maranzano, N.J. Wagner, J. Chem. Phys. **117**, 10291 (2002)
17. N.J. Wagner, J.F. Brady, Phys. Today **62**, 27 (2009)
18. X. Cheng, J.H. McCoy, J.N. Israelachvili, I. Cohen, Science **333**, 1276 (2011)
19. Y.S. Lee, N.J. Wagner, Rheol. Acta **42**, 199 (2003)
20. C. Fischer, C.J.G. Plummer, V. Michaud, P.E. Bourban, J.A.E. Manson, Rheol. Acta **46**, 1099 (2007)
21. V.S. Deshpande, N.A. Fleck, Int. J. Impact Eng. **24**, 277 (2000)
22. T.S. Lok, P.J. Zhao, J. Mater. Civ. Eng. **16**, 54 (2004)
23. C. Bo, J. Balzer, K.A. Brown, S.M. Walley, W.G. Proud, Eur. Phys. J. Appl. Phys. **55**, 31201 (2011)
24. K. Ogawa, J. Phys. IV **110**, 435 (2003)
25. A.S. Lim, S.L. Lopatnikov, J.W. Gillespie, Polym. Test **28**, 891 (2009)
26. A.S. Lim, S.L. Lopatnikoy, N.J. Wagner, J.W. Gillespie, J. Non-Newton. Fluid Mech. **166**, 680 (2011)
27. B.O. Ahrstrom, S. Lindqvist, E. Hoglund, K.G. Sundin, Proc. Inst. Mech. Eng. Part J. Journal of Engineering Tribology **216**, 63 (2002)
28. E.V. Lomakin, P.A. Mossakovsky, A.M. Bragov, A.K. Lomunov, A.Y. Konstantinov, M.E. Kolotnikov, F.K. Antonov, M.S. Vakshtein, Arch. Appl. Mech. **81**, 2007 (2011)
29. B. Song, W. Chen, Exp. Mech. **44**, 300 (2004)
30. G. Ravichandran, G. Subhash, J. Am. Ceram. Soc. **77**, 263 (1994)
31. D.J. Frew, M.J. Forrestal, W. Chen, Exp. Mech. **42**, 93 (2002)
32. D.J. Frew, M.J. Forrestal, W. Chen, Exp. Mech. **45**, 186 (2005)
33. O.E. Petel, A.J. Higgins, J. Appl. Phys. **108**, 114918 (2010)
34. M.A. Meyers, *Dynamic Behavior of Materials*, 1st edn. (Wiley, New York, 1994)